Molecular architecture of human prion protein amyloid: A parallel, in-register β-structure

Nathan J. Cobb*, Frank D. Sönnichsen*, Hassane Mchaourab†, and Witold K. Surewicz*‡

*Department of Physiology and Biophysics, Case Western Reserve University, Cleveland, OH 44106; and †Department of Molecular Physiology and Biophysics, Vanderbilt University Medical Center, Nashville, TN 37232

Edited by Reed B. Wickner, National Institutes of Health, Bethesda, MD, and approved October 3, 2007 (received for review July 11, 2007)

Transmissible spongiform encephalopathies (TSEs) represent a group of fatal neurodegenerative diseases that are associated with conformational conversion of the normally monomeric and α-helical prion protein, PrP^C, to the β-sheet-rich PrP^{Sc}. This latter conformer is believed to constitute the main component of the infectious TSE agent. In contrast to high-resolution data for the PrP^C monomer, structures of the pathogenic PrP^{Sc} or synthetic PrP^{Sc}-like aggregates remain elusive. Here we have used site-directed spin labeling and EPR spectroscopy to probe the molecular architecture of the recombinant PrP amyloid, a misfolded form recently reported to induce transmissible disease in mice overexpressing an N-terminally truncated form of PrP^C. Our data show that, in contrast to earlier, largely theoretical models, the conformational conversion of PrP^C involves major refolding of the C-terminal α-helical region. The core of the amyloid maps to C-terminal residues from ≈160–220, and these residues form single-molecule layers that stack on top of one another with parallel, in-register alignment of β-strands. This structural insight has important implications for understanding the molecular basis of prion propagation, as well as hereditary prion diseases, most of which are associated with point mutations in the region found to undergo a refolding to β-structure.

EPR | spin labeling | transmissible spongiform encephalopathy

Transmissible spongiform encephalopathies (TSEs), commonly referred to as prion diseases, represent a group of fatal neurodegenerative disorders that arise in several mammalian species by either sporadic, inherited, or infectious means. These disorders include bovine spongiform encephalopathy in cattle, scrapie in sheep, chronic wasting disease in cervids, and Creutzfeldt–Jakob disease and kuru in humans (1–6). In recent years, TSEs have drawn much attention from both scientists and the public because of the epidemics of bovine spongiform encephalopathy and indications that this disease might be infectious to humans (2, 4).

The prion disorders, like Alzheimer's and Parkinson's diseases, are associated with neuronal accumulation of abnormal protein deposits, often composed of amyloid fibrils. In the case of TSEs, these aggregates result from the conversion of the normal cellular prion protein, PrP^C, to an abnormal conformer, PrP^{Sc} (1–6). The protein-only hypothesis asserts that the transmission of TSEs does not require nucleic acids, and that PrP^{Sc} represents a self-perpetuating infectious agent (1, 2). Once heretical, this model is now gaining rapid acceptance (1–7), especially in view of recent advances in generating infectious PrP^{Sc} *in vitro* (8–10). In a more general context, the prion concept is strongly supported by studies of protein conformation-based inheritance in yeast and other fungi (11–13).

Cellular human PrP^C is a 209 residue glycoprotein with a C-terminally attached glycosylphosphatidylinositol anchor (2–5). It consists of a flexible N-terminal region and a C-terminal globular domain comprised of three α-helices and two short β-strands, with a disulfide bond bridging helices 2 and 3 (14–16). Although PrP^C and PrP^{Sc} appear to share the same covalent structure, they differ profoundly in biophysical properties. PrP^C is monomeric, proteinase K (PK)-sensitive, and soluble in nonionic detergents, whereas PrP^{Sc} is partially resistant to PK digestion and insoluble, forming aggregates with characteristics often similar to amyloid fibrils (1–6). Furthermore, optical spectroscopic data indicate that the $PrP^C \rightarrow PrP^{Sc}$ conversion is accompanied by a marked increase in β-sheet structure (17, 18).

In contrast to the high-resolution data for the PrP^C monomer (14–16), the structure of PrP^{Sc} (and PrP^{Sc}-like aggregates) is largely unknown. This critical gap in TSE research largely reflects experimental difficulties in structural studies of large protein aggregates such as amyloid fibrils. Our recent hydrogen/deuterium (H/D) exchange study has provided an initial low-resolution insight into the location of the β-sheet core in the recombinant PrP amyloid (19). However, the molecular architecture of this core region remains unknown.

Here we have used site-directed spin labeling (SDSL), coupled with EPR spectroscopy, to obtain residue-specific information about the organization of individual PrP molecules within the amyloid fibrils formed by the recombinant human PrP90–231 (huPrP90–231). This fragment, corresponding to synthetic prions used in infectivity studies of Legname *et al.* (8), encompasses the entire PK-resistant sequence of brain PrP^{Sc}, is sufficient for propagation of disease, and contains all known point mutations associated with hereditary prion disorders (2, 4). Our present investigation was conducted by using D178N huPrP90–231. This largely disease-associated variant undergoes an especially efficient autocatalytic conversion to the amyloid state, facilitating conversion of PrP mutants harboring the nonnative, nitroxide-labeled cysteines required for SDSL analysis (20). In contrast to existing, theoretical models (21, 22), our results demonstrate that the core of the amyloid maps to the C-terminal part of the protein, and that residues within this region form single-molecule layers that stack on top of each other with parallel, in-register alignment of β-strands.

Results

The main advantage of the SDSL approach is that spin interactions allow for distance estimates between nitroxide labels (23, 24). Thus, if a single label is present on each protein molecule, EPR spectra provide crucial information about quaternary structure within the amyloid fibril (i.e., intermolecular contact sites and packing of individual protein monomers). Typically, spin–spin interactions between nitroxide labels in proteins are dominated by dipolar effects that result in a broadening of EPR spectra, providing distance information in the range of ≈8–25 Å

Author contributions: N.J.C. and W.K.S. designed research; N.J.C. performed research; N.J.C., F.D.S., H.M., and W.K.S. analyzed data; and N.J.C., F.D.S., and W.K.S. wrote the paper.

The authors declare no conflict of interest.

This article is a PNAS Direct Submission.

Freely available online through the PNAS open access option.

‡To whom correspondence should be addressed. E-mail: witold.surewicz@case.edu.

This article contains supporting information online at www.pnas.org/cgi/content/full/0706522104/DC1.

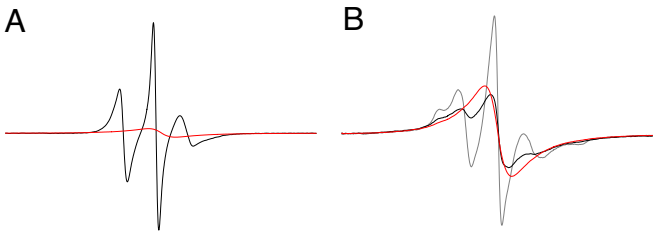

Fig. 1. Spin exchange in prion amyloid fibrils. (*A*) EPR spectra for the representative huPrP90–231 variant spin labeled at position 188 in the monomeric (black line) and fibrillized (red line) forms. (*B*) EPR spectra for amyloid fibrils generated by using labeled protein alone (red line) and mixtures of labeled and unlabeled protein at a 1:1 ratio (black line) and 1:4 ratio (gray line). Spectra within each panel (but not between panels) are normalized to the same number of spins, and for visualization purposes, each panel is scaled to the same vertical size. Scan width is 150 G.

(23, 24). A second type of interaction, spin exchange, occurs at much smaller distances, when on the EPR time scale ($<10^{-7}$ s) multiple nitroxide labels are in sufficient proximity to allow orbital overlap (25–27). This type of interaction strikingly reduces classical three-line EPR spectra to a single feature. Regardless of proximity, the presence of just two labels is insufficient to result in a single-line EPR spectrum (26–28), making these signals extremely unusual in proteins. However, spectra such as these have recently been reported for spin-labeled fibrils formed by tau (26) and α-synuclein (27).

PrP Amyloid Core and Its Packing Motif. For the present structural study, we prepared nearly 50 nitroxide-derivatized Cys mutants of huPrP90–231. EPR signals obtained for these labeled proteins in solution showed classical three-line spectra (Fig. 1*A*), consistent with monomeric protein. Incubation of each of these proteins under the conditions described in *Materials and Methods* resulted in thioflavine T-positive amyloid fibrils as verified by fluorescence spectroscopy, atomic force microscopy, and electron microscopy (EM) (20). Inspection of EPR signals revealed dramatic differences between residues in different regions of the amyloid (Fig. 2). Remarkably, nearly two-thirds of the 31 variants with nitroxide labels within the ≈160–220 region were found to possess single (or nearly single)-line spectra. As discussed above, spectra of this type are indicative of extensive spin exchange, implying close proximity of nitroxide radicals. Consistent with this interpretation (26, 27), generation of mixed fibrils containing 50% unlabeled protein resulted in a loss of signal amplitude because interspin distances increase and spectra become affected by dipolar broadening (Fig. 1*B*). An increase in the amplitude was observed only upon further dilution with unlabeled protein, when larger interspin distances diminish even dipolar interactions (Fig. 1*B*).

Single-line EPR signals are commonly associated with crystals or highly concentrated solutions of nitroxide radicals, where the frequent interaction of paramagnetic centers is due to either tight packing or transient collisions (25). To probe the nature of these interactions in PrP amyloid fibrils, we measured EPR spectra at low temperatures. Even at 150 K, the single-line character was maintained [supporting information (SI) Fig. 5], clearly indicating that the spin exchange observed in our study

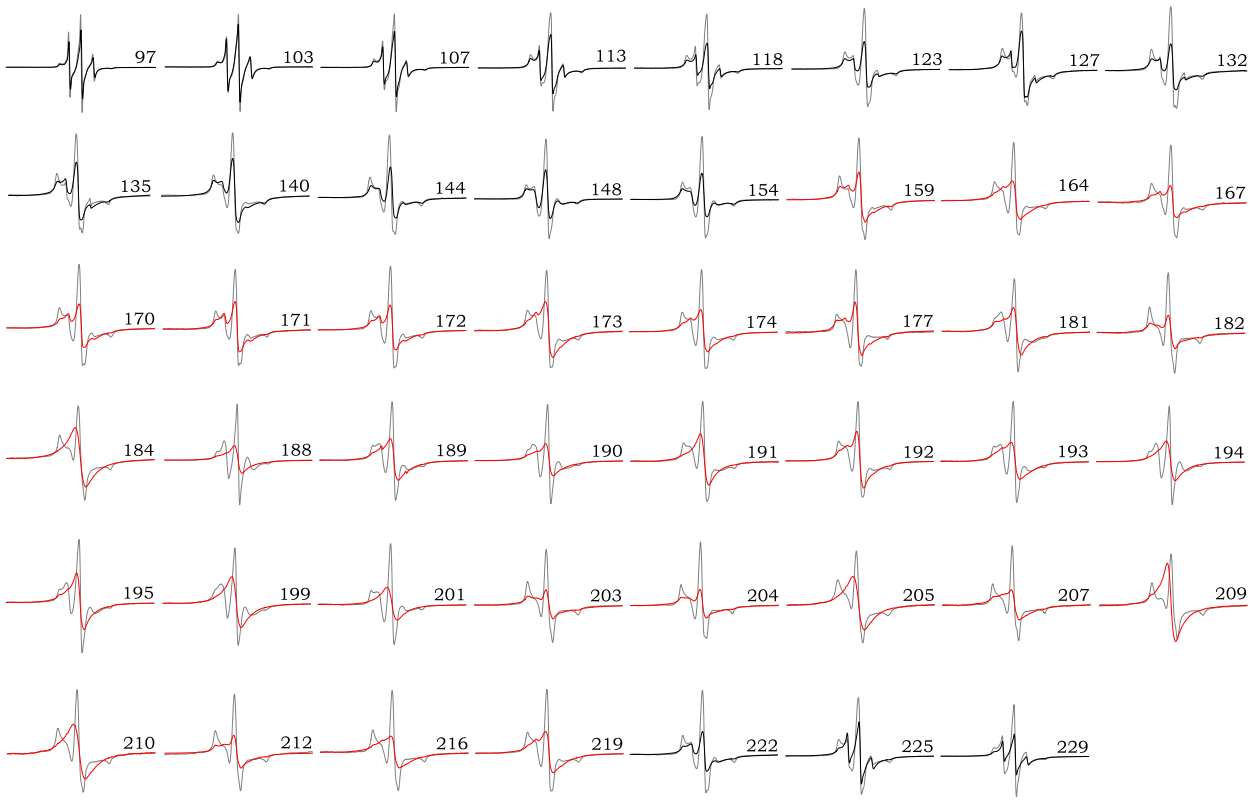

Fig. 2. EPR signals obtained from fibrils generated by using D178N huPrP 90–231 labeled at indicated positions. For clarity of presentation, spectra displaying a high degree of spin exchange are shown in red, and those spectra affected largely by dipolar broadening are shown in black. Spectra for spin-diluted fibrils generated by using a 1:4 ratio of labeled to unlabeled protein are shown as gray lines. Scan width is 200 G, and spectral pairs for each site are scaled to the same number of spins.

was not due to rapid motional fluctuations resulting in frequent internitroxide contact. Thus, spin labels attached to PrP within the region spanning sites ≈160–220 must form a tightly packed network, in which each label is in close proximity to its counterparts on neighboring molecules.

In the native structure of the PrP monomer, residues 160–220 encompass helix 2, a major part of helix 3, and the loop between these two helices (14–16). This α-helical arrangement certainly cannot accommodate the direct contact of consecutive positions in adjacent molecules as was observed in this study (best evidenced for residues 188–195). Consistent with the established increase in β-structure content upon conversion to amyloid (20, 29), the only scenario compatible with the present data is that residues within this "core" region stack as single molecule layers with close proximity of same residues in the adjacent PrP molecules. The location of this tightly packed β-sheet region correlates remarkably well with recent H/D exchange studies conducted in our laboratory (19), which mapped an exchange-protected core to residues ≈169–221.

As extensively discussed in previous studies (26, 27), single-line spectra such as those observed for the core region of the PrP amyloid are strongly indicative of parallel, in-register organization of the stacked β-strands, in which the distance between same sites is ≈4.8 Å. Indeed, while one could argue whether the upper distance limit between nitroxide radicals required to produce spectra of this type is 5 or 6 Å, this limit is certainly less than the ≈9.6 Å distance expected for an antiparallel arrangement. To further probe this issue, a series of spin dilution experiments was performed, in which mixed fibrils were formed with increasing proportions of unlabeled protein. Again, the effect of dilution on EPR spectra was consistent only with parallel stacking of PrP monomers (see SI Fig. 6 and legend).

Can this parallel alignment of β-strands be other than in-register? A one residue displacement from perfect registry would position nitroxide labels on opposite sides of a β-sheet, with large internitroxide distances (≈14 Å) across the strand that are incompatible with single-line spectra. Indeed, experiments using fibrils formed by a 1:1 comixture of proteins labeled at sequential residues along this stretch (i.e., *i* and *i* + *1* or *i* and *i* − *1*) revealed a loss of spin exchange, as indicated by the appearance of hyperfine splittings (SI Fig. 7). A two residue displacement from perfect registry would result in labels positioned on the same side of the sheet, but with nearest nitroxide neighbors ≈8 Å apart. As discussed above, this distance is still considerably longer than that required for single-line spectra. We could not examine proteins labeled at all sites within the ≈160–220 region because some Cys mutants failed to purify (presumably due to incorrect disulfide pairing). Therefore, one cannot completely discount the possibility of a small displacement from a perfect in-register arrangement within some parts of this region. However, the existence of a great many interspersed single-line spectra (Fig. 2) is most consistent with an in-register stacking motif within the entire core region.

Some labeled residues within the ≈160–220 core region display EPR signals showing less than perfect spin exchange (Fig. 2). Although these spectra are somewhat less unambiguous in their interpretation, they are certainly not inconsistent with our proposed parallel, in-register packing motif of the PrP amyloid. Similar EPR signals have been observed previously for spin-labeled Aβ fibrils (30), and these amyloid structures were shown by NMR to adopt parallel and in-register alignment of β-strands (31, 32). An intrinsic caveat of all spin-labeling studies of proteins relates to the presence of a relatively bulky nitroxide label that can (and often does) introduce local structural perturbation, with a degree of this perturbation depending largely on steric interactions with neighboring side chains. Within parallel β-structure, insufficient packing space for nitroxides at some positions could result in a "staggering" of these large side chains, preventing perfect orbital overlap and reducing the efficiency of spin exchange. Thus, any model derived from EPR data must be based on a prevailing trend emerging from examining spectra at many different sites. In this context, we were fortunate to successfully introduce spin labels at so many positions displaying highly unique single-line spectra. In accord with the interpretation of previous spin labeling studies for tau and α-synuclein (26, 27), we conclude that the single-line spectra observed in the present study reflect a parallel and in-register packing motif within the core of the PrP amyloid fibril.

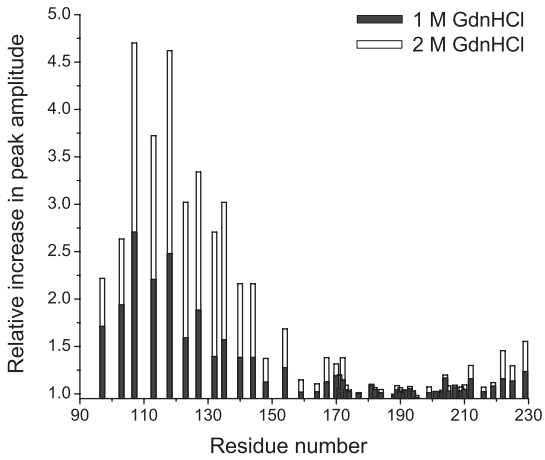

Fig. 3. Changes in central line amplitude for EPR spectra of fibrils resuspended in 1 and 2 M GdnHCl relative to the amplitude in the absence of denaturant. Spectra for sites ≈160–220 show little change, and thus the molecular architecture of this region is maintained in the presence of the denaturant. Residues N-terminal to 160 display particularly large increases in amplitude, indicating low stability of any structure in this region to chemical denaturation. Relatively small responses observed for the most N-terminal sites (97 and 103) are due to already large interspin distances and mobilities of these sites in the absence of denaturant (see Fig. 2).

Outside residues ≈160–220, no spectrum for PrP amyloid displayed evidence of spin exchange, although most indicated modest dipolar broadening (Fig. 2). Spectra for some of these sites, especially in the N-terminal region, showed marked heterogeneity with at least two populations of differing mobility. This is evidenced by multiple features of the central line, as well as a sharp component present in the downfield peak. Multiple nitroxide populations complicate precise distance measurements by standard deconvolution methods (23, 24). Nevertheless, it is clear that sites outside the ≈160–220 core region do not possess the tight packing and high degree of order required for efficient spin exchange, and for all of them interspin distances are calculated to be >13 Å (for sites N-terminal to 118 above 17 Å).

The Core Region Represents a Single Cooperative Domain. To build on our understanding of the amyloid core, a series of GdnHCl titrations were performed with the spin-labeled fibrils. Any denaturant-induced loss of structure would be expected to result in greater signal amplitude due to increased mobility and larger interspin distances. Fig. 3 shows that, for the vast majority of residues within the region characterized by spin exchanged spectra, there is little increase in signal amplitude at GdnHCl concentrations up to at least 2 M, indicating that the integrity of the highly ordered structure is maintained. In stark contrast, spectra for sites outside this region show amplitude increases of up to several fold, clearly demarcating the stable core of the amyloid. At denaturant concentrations >2 M, equilibrium with dissociated monomeric protein resulted in EPR spectra contaminated with a highly mobile component (SI Fig. 8). However, for the core residues, subtraction of this mobile component resulted

in the fully spin exchanged (single-peak) spectrum, revealing that the molecular organization of the core region in remaining fibrils is unchanged (SI Fig. 8). Altogether, these experiments indicate that the ≈160–220 region represents a single cooperative domain, and that unfolding of this core is intimately associated with fibril dissociation into individual PrP monomers.

Effect of Fibril Annealing on EPR Spectra. Amyloid fibrils produced by recombinant PrP are characterized by a shorter PK-resistant core relative to brain PrP^{Sc} (29). However, it was recently found that by annealing synthetic fibrils at high temperatures in the presence of Triton X-100, this PK resistance increases, although not quite to the levels observed for PrP^{Sc} (19, 29). The present SDSL analysis indicates that only residues from ≈100–135 are affected by this process, with EPR spectra generally becoming more homogeneous (SI Fig. 9). Although annealing results in modest site-specific changes in nitroxide environment, we found no evidence for any N-terminal extension of the stacked β-core as defined by high degree of spin exchange (SI Fig. 9). This finding is fully consistent with our recent H/D exchange study, further reinforcing the notion that PK-resistant regions of amyloid fibrils are not necessarily limited to highly ordered β-structure and also may result from steric constraints imposed by tertiary interactions (19).

Discussion

One of the most enduring mysteries in the TSE field is the structure of the infectious PrP^{Sc} form of the prion protein. Because high-resolution structural studies with brain-derived PrP^{Sc} remain outside the reach of currently available methods, the most–if not only–practical way to address this problem is to resort to PrP^{Sc}-like aggregates formed *in vitro* by the recombinant PrP. Of particular relevance in this respect is fibrillar amyloid, a misfolded form of PrP reported to cause a transmissible neurological disorder in transgenic mice overexpressing PrP^{C} (8). Even in the case of these synthetic prions, however, the structural analysis presents a major experimental challenge. Previous attempts in this regard were limited to global topological studies by using digital reconstitution of electron micrographs of fibrils formed from PrP monomers lacking the native disulfide bond (33). One of few techniques suitable for a higher resolution analysis is site-directed spin labeling (26, 27, 30). Using this approach, here we have determined that the core of the PrP amyloid is located within the C-terminal region encompassing residues ≈160–220. Most important, the present data allowed us to identify the major folding motif for the PrP amyloid, demonstrating that residues within the core region form single molecule layers that stack on top of one another with parallel and in-register alignment of β-strands.

A parallel, in-register β-sheet structure appears to be a common motif for many amyloids, including Aβ (30–32), α-synuclein (27), tau (26), and the yeast prion proteins Ure2p (42) and Sup35 (34), although for the latter protein an alternative, β-helix-like model has also been proposed (35). Recent crystallographic studies have provided atomic-level insight into the organization of β-strands in microcrystals formed by short (4–7 residue) synthetic peptides corresponding to segments of amyloidogenic proteins (36, 37). This work identified a common "steric zipper" motif, whereby pairs of β-sheets form a dry interface with interdigitation of side chains. However, similar crystallographic studies for longer polypeptides are not yet feasible. Thus, with the notable exception of the extensively studied Aβ peptide (30–32), structural models for amyloids formed by larger, biologically relevant proteins are general and of low resolution.

Our present experimental data also fall short of directly providing atomic-level details, such as directionality of individual amino acid side chains or the precise topology of β-strands. However, in the case of PrP amyloid, a special constraint is imposed by the presence of a native disulfide bridge between cysteines 179 and 214, requiring specific looping and limiting the number of possible PrP amyloid structures. The length of this loop region (34 residues) implies the existence of bulges, which shorten the β-strands found within it. The location of these tight turns can be modeled to reduce the number of charged residues in the dry intersheet interface, where unfavorable electrostatic forces between like charges cannot be shielded by solvent interactions.

The simplest model based on the β-stacking motif determined herein is one in which the backbone bends in β-bulges near the disulfide bridge (SI Fig. 10*A*). Although the precise location of these bulges is somewhat arbitrary, we model one of them at position 181 because the respective asparagine is highly compatible with the positive phi-angle of the bend. A major drawback to this model, however, is that it places three charged residues (one lysine and two glutamic acids) in the dry intersheet interface, making such a structure thermodynamically unstable. The above problem largely disappears in a model where a second pair of β-bulges is introduced within the disulfide bridged loop (Fig. 4 and SI Fig. 10*B*). This latter structure has only one charged residue (Glu 211) within the dry interface. This residue can hydrogen bond to (Gln 186), resulting in a more polar local environment and thereby reducing unfavorable intermolecular electrostatic interactions. Thus, the structure depicted in Fig. 4 is energetically far more plausible. For comparison, a generally accepted structural model for Aβ amyloid has two charged residues in a dry interface, where intermolecular repulsions between like charges are partially neutralized by a salt bridge (31, 32). The dimensions of the present structural model (≈10 × 3.5 nm) easily fit within the apparent width (12 ± 1 nm) of PrP amyloid fibrils as observed by EM (Fig. 4*B*). However, our data cannot discern whether mature PrP fibrils are comprised of one or two tightly packed individual filaments.

While the recombinant protein used in this study is devoid of any post-translational modifications, brain PrP can be glycosylated at residues N181 and N197. Although recombinant amyloid would not be influenced by such steric constraints, any structural model approximating the brain PrP amyloid must position side chains of these residues to the outside of the intercysteine loop. Situated at the approximate midpoint of this loop, N197 is located at the most likely bend of the amyloid fold, where its directionality is relatively unrestrained. Furthermore, the β-bulge modeled at N181 orients its side chain outward to accommodate the bulky sugars present in brain PrP. Thus, our model also would be compatible with glycosylated PrP amyloid.

The two most prominent models previously proposed for the structure of PrP amyloid are the β-helix fold (21) and the spiral model (22). The former, obtained by threading a portion of the PrP sequence through a known β-helix fold, postulates that the core of the amyloid consists of residues 89–175 forming left-handed β-helices, with the C-terminal α-helices 2 and 3 of PrP^{C} largely preserved. In contrast, the spiral model, derived from molecular dynamics simulations, proposes that the core consists of parallel and antiparallel β-strands within the 116–164 region, allowing all three α-helices to retain their native conformation. Our present experimentally derived architecture of PrP amyloid, in which the entire region encompassing the two C-terminal α-helices in PrP^{C} refolds into intermolecularly hydrogen-bonded β-strands, is fundamentally different from both of these *in silico* models, both with respect to the location of the β-core as well as the folding motif within this core region. Remarkably, residues involved in β-stacking as determined herein by the SDSL method correspond closely to those recently found to be protected against H/D exchange (19). This striking consistency further supports our conclusions regarding the PrP core region.

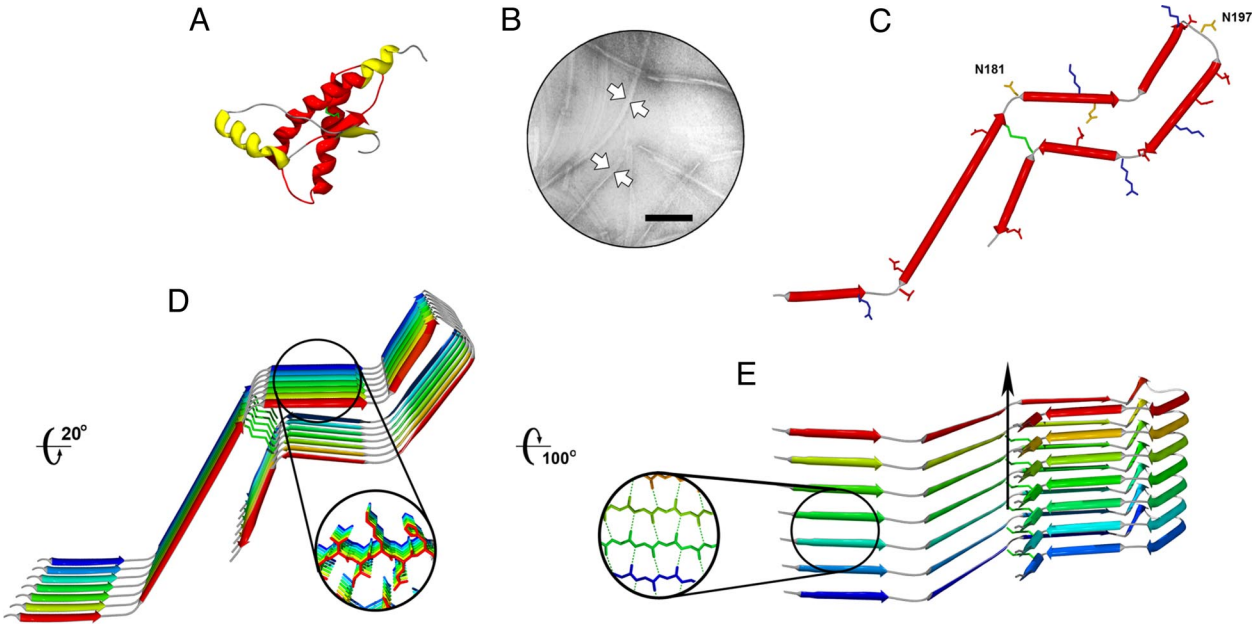

Fig. 4. The simplest model of recombinant PrP amyloid consistent with present experimental data. (*A*) The monomeric folded domain (residues 120–231) of human PrP. Residues determined herein to form the core of the amyloid are highlighted in red. (*B*) Electron micrograph of PrP amyloid fibrils. (Scale bar: 100 nm.) The width of the fibrils (arrows) was determined to be 12 ± 1 nm. (*C*) Model for the fold of the PrP amyloid core (residues 159–219) consistent with the present data. The native disulfide bond is shown in green, charged residues are colored red (negative) and blue (positive), and potential N-linked glycosylation sites are labeled. The only charged residue positioned in the dry interface, E211, is in hydrogen-bonding distance of Q186. The exact identity of β-strands is unknown, and orientation of the most N-terminal strands is arbitrary. (*D*) In-register stacking motif of nearly planar PrP monomers in the amyloid modeled with tight interdigitation of the side chains. (*E*) Rotated structure showing the network of intermolecular hydrogen bonding. The arrow indicates the long axis of the fibril.

While synthetic amyloid fibrils similar to those used in the present study have been shown to induce a TSE-like disease in mice overexpressing PrP89–231, the infectivity titer was low (8). Recent work by Legname *et al.* (38) demonstrated that PrP^{Sc} isolates of low conformational stability display the highest infectivity, suggesting that a highly stable, "slow" strain is adopted by the recombinant PrP amyloid. An alternative possibility, however, is that only a small population of synthetic aggregates adopts a structure representing that of the true infectious agent. Additionally, it has been shown that highest infectivity per mass unit is associated with prion particles substantially smaller than long amyloid fibrils (39). However, as pointed out by the authors themselves, this does not necessarily imply structural differences at the molecular level, as higher specific infectivity of smaller particles might be simply due to the larger number of ends available for the recruitment of the PrP^{C} monomer. How well then does the molecular architecture for recombinant PrP amyloid fibrils determined here relate to infectious brain-derived PrP^{Sc}? While it seems unlikely that the spontaneously adopted parallel stacking of residues ≈160–220 observed within synthetic PrP fibrils does not describe this region's overall folding motif within PrP^{Sc}, one cannot absolutely discount this possibility. Furthermore, compared with their brain-derived counterparts, synthetic PrP fibrils display reduced PK resistance for residues ≈90–150 (19, 29). This suggests some PrP^{Sc}-specific structural arrangement within this region which is not fully recapitulated in synthetic amyloid fibrils. Clearly, a host of cellular factors could modulate both the infectivity and structure of misfolded PrP aggregates. Nevertheless, the elucidation of the molecular architecture of the synthetic PrP amyloid conformer represents a major advance in the field, at the least providing a necessary "baseline" for interpretation of any inherently low-resolution constraints obtained for brain-derived PrP^{Sc}.

Apart from providing a long-sought structural basis for understanding the mechanism of mammalian prion propagation, the present findings also may help explain the enigma of hereditary prion diseases, in which the pathogenic process appears to develop spontaneously in the absence of any exogenous infectious agents. Remarkably, the vast majority of point mutations associated with these disorders map to the region found herein to undergo a transition to β-structure (4). Thus, these mutations are well positioned to cause structural and/or thermodynamic perturbation of this critical region in PrP^{C} (40), thereby facilitating the spontaneous conversion to the PrP^{Sc} isoform. The present structural model may also offer a rationale for baffling findings that the pattern of glycosylation (i.e., the ratio of diglycosylated, monoglycosylated, and unglycosylated PrP) is one of the determinants of prion strain diversity, being fatefully propagated upon transmission (2, 4). Tight packing of monomers in PrP amyloid dictates that, in glycosylated protein, highly flexible but bulky glycans attached to the same glycosylation sites on nearby molecules would have to spread in different directions. However, steric clashes between sugar moieties would likely result in a perturbation and/or destabilization of the highly ordered structure determined herein for unglycosylated PrP. By affecting the extent of this perturbation, the ratio of glycoforms may subtly modulate the PrP^{Sc} conformation, resulting in an aggregate that preferentially recruits monomers with similar glycoform ratios. Thus, these structural effects could explain glycosylation-dependent strain diversity, in line with current thinking that prion strains are fully encoded in distinct conformations of ordered protein aggregates (2, 11, 13, 35, 41).

Materials and Methods

Generation of Spin-Labeled Cysteine Variants and Protein Purification. Cysteine variants of the 6×His-tagged D178N huPrP90–231 construct were generated by site-directed mutagenesis, and all

proteins were expressed and subjected to our initial Ni-NTA purification and refolding procedure as described in ref. 20. Unfortunately, introduction of non-native cysteine resulted in nonspecific aggregation of some variants during this process. Most mutants were found to refold correctly and purify, however, and stocks of unlabeled protein were incubated overnight with a 5-fold molar excess of the disulfide-specific reducing agent, Tris(2-carboxyethyl)phosphine hydrochloride. Next, the protein was diluted with 50 mM potassium phosphate buffer (pH 7.6), filtered, and incubated with a 10-fold molar excess of the MTSL spin-labeling reagent ([1-oxy-2,2,5,5-tetramethyl-pyrolline-3-methyl]-methanethiosulfonate) and thrombin (10 units/mg of protein) for 5 h at room temperature. The extent of 6×His-tag cleavage and nitroxide labeling was determined by mass spectrometry, and incubation was continued if necessary until full labeling and cleavage were observed. Final purification of the now-labeled protein was performed on a CM-Sepharose column (20). Far-UV circular dichroism spectra of all purified variants were essentially identical, revealing native α-helical structure. To verify native disulfide formation, labeled variants were subjected to digestion with pepsin, and the resulting fragments were analyzed by mass spectrometry as described in ref. 19.

Preparation of Amyloid Fibrils. Generation of amyloid fibrils using labeled protein was performed as described in the previous study (19). The conversion process was followed using a fluorometric thioflavin T assay and atomic force microscopy (20, 41). Furthermore, fibrils were visualized by transmission EM (JEOL 1200EX instrument) using Formvar/carbon-coated grids and negative staining with uranyl acetate. Freshly prepared samples were pelleted by centrifugation and washed three times with 50 mM potassium phosphate buffer (pH 7.5) to remove any monomeric protein or soluble aggregates. The washed pellet was finally resuspended in 30 μl of the same buffer and loaded into a capillary. After the initial EPR signal was obtained, samples were removed from the capillary tube, subjected to the annealing process as described in ref. 19, and again analyzed by EPR spectroscopy. For denaturation studies, samples were diluted into 50 mM potassium phosphate buffer (pH 7.5) containing increasing amounts of GdnHCl (0.5–6 M) and allowed to equilibrate for 30 min before EPR measurement.

EPR Spectroscopy. EPR spectra were measured at room temperature using a Bruker EMX spectrometer fitted with the high-sensitivity probehead. Power was set to 12 mW, with a scan width of 200 G unless otherwise noted. Field modulation was varied from 1 to 2 G depending on the degree of spin label immobilization. When applicable, spectra in the dipolar broadening regime were analyzed to obtain interspin distance estimates using a previously described methodology (23). Spectra within individual panels were normalized to the same number of spins. For clarity of display, each panel was scaled to the same amplitude.

This work was supported by National Institutes of Health (NIH) Grants NS 44158 and NS 38604 (to W.K.S.). N.J.C. acknowledges support from NIH Training Grant T32 HL07653.

1. Prusiner SB (1982) *Science* 216:136–144.
2. Prusiner SB (1998) *Proc Natl Acad Sci USA* 95:13363–13383.
3. Caughey B, Baron GS (2006) *Nature* 443:803–810.
4. Collinge J (2001) *Annu Rev Neurosci* 24:519–550.
5. Aguzzi A, Polymenidou M (2004) *Cell* 116:313–327.
6. Weissmann C (2004) *Nat Rev Microbiol* 2:861–871.
7. Surewicz WK, Jones EM, Apetri AC (2006) *Acc Chem Res* 39:654–662.
8. Legname G, Baskakov IV, Nguyen HO, Riesner D, Cohen FE, DeArmond SJ, Prusiner SB (2004) *Science* 305:673–676.
9. Castilla J, Saa P, Hetz C, Soto C (2005) *Cell* 121:195–206.
10. Deleault NR, Harris BT, Rees JR, Supattapone S (2007) *Proc Natl Acad Sci USA* 104:9741–9746.
11. Chien P, Weissman JS, DePace AH (2004) *Annu Rev Biochem* 73:617–656.
12. Uptain SM, Lindquist S (2002) *Annu Rev Microbiol* 56:703–741.
13. Wickner RB, Edskes HK, Roberts BT, Baxa U, Pierce MM, Brachmann A (2007) *Genes Dev* 18:470–485.
14. Riek R, Hornemann S, Wider G, Billeter M, Glockshuber R, Wuthrich K (1996) *Nature* 382:180–182.
15. Zahn R, Liu A, Luhrs T, Riek R, von Schroetter C, Lopez Garcia F, Billeter M, Calzolai L, Wider G, Wuthrich K (2000) *Proc Natl Acad Sci USA* 97:145–150.
16. Donne DG, Viles JH, Groth D, Mehlhorn I, James TL, Cohen FE, Prusiner SB, Wright PE, Dyson HJ (1997) *Proc Natl Acad Sci USA* 94:13452–13457.
17. Caughey BW, Dong A, Bhat KS, Ernst D, Hayes SF, Caughey WS (1991) *Biochemistry* 30:7672–7680.
18. Pan KM, Baldwin M, Nguyen J, Gasset M, Serban A, Groth D, Mehlhorn I, Huang Z, Fletterick RJ, Cohen FE, *et al.* (1993) *Proc Natl Acad Sci USA* 90:10962–10966.
19. Lu X, Wintrode PL, Surewicz WK (2007) *Proc Natl Acad Sci USA* 104:1510–1515.
20. Apetri AC, Vanik DL, Surewicz WK (2005) *Biochemistry* 44:15880–15888.
21. Govaerts C, Wille H, Prusiner SB, Cohen FE (2004) *Proc Natl Acad Sci USA* 101:8342–8347.
22. DeMarco ML, Daggett V (2004) *Proc Natl Acad Sci USA* 101:2293–2298.
23. Altenbach C, Oh KJ, Trabanino RJ, Hideg K, Hubbell WL (2001) *Biochemistry* 40:15471–15482.
24. Xiao WS, Shin Y-K (2000) in *Biological Magnetic Resonance*, eds Berliner LJ, Eaton GR, Eaton SS (Kluwer, New York), pp 249–276.
25. Molin YN, Salikhov KM, Zamaraev KI (1980) *Spin Exchange*: *Principles and Applications in Chemistry and Biology* (Springer, Berlin).
26. Margittai M, Langen R (2004) *Proc Natl Acad Sci USA* 101:10278–10283.
27. Chen M, Margittai M, Chen J, Langen R (2007) *J Biol Chem* 282:24970–24979.
28. Langen R, Oh KJ, Cascio D, Hubbell WL (2000) *Biochemistry* 39:8396–8405.
29. Bocharova OV, Makarava N, Breydo L, Anderson M, Salnikov VV, Baskakov IV (2006) *J Biol Chem* 281:2373–2379.
30. Török M, Milton S, Kayed R, Wu P, McIntire T, Glabe CG, Langen R (2002) *J Biol Chem* 277:40810–40815.
31. Petkova AT, Ishii Y, Balbach JJ, Antzutkin ON, Leapman RD, Delagio F, Tycko R (2002) *Proc Natl Acad Sci USA* 99:16742–16747.
32. Lührs T, Ritter C, Adrian M, Riek-Loher D, Bohrmann B, Döbeli H, Schubert D, Riek R (2005) *Proc Natl Acad Sci USA* 102:17342–17347.
33. Tattum MH, Cohen-Krausz S, Thumanu K, Wharton CW, Khalili-Shirazi A, Jackson GS, Orlova EV, Collinge J, Clarke AR, Saibil HR (2006) *J Mol Biol* 357:975–985.
34. Shewmaker F, Wickner RB, Tycko R (2006) *Proc Natl Acad Sci USA* 103:19754–19759.
35. Krishnan R, Lindquist SL (2005) *Nature* 435:765–772.
36. Nelson R, Sawaya MR, Balbirnie M, Madsen AØ, Riekel C, Grothe R, Eisenberg D (2005) *Nature* 435:773–778.
37. Sawaya MR, Sambashivan S, Nelson R, Ivanova MI, Sievers SA, Apostol MI, Thompson MJ, Balbirnie M, Wiltzius JJW, McFarlane HT, *et al.* (2007) *Nature* 447:453–457.
38. Legname G, Nguyen HO, Peretz D, Cohen FE, DeArmond SJ, Prusiner SB (2006) *Proc Natl Acad Sci USA* 103:19105–19110.
39. Silveira JR, Raymond GJ, Hughson AG, Race RE, Sim VL, Hayes SF, Caughey B (2005) *Nature* 437:257–261.
40. Apetri AC, Surewicz K, Surewicz WK (2004) *J Biol Chem* 279:18008–18014.
41. Jones EM, Surewicz WK (2005) *Cell* 121:63–72.
42. Kajava AV, Baxa U, Wickner RB, Steven AC (2004) *Proc Natl Acad Sci USA* 101:7885–7890.